Supplementary Information For

Polysulfides intercalation in bilayer structured graphitic C_3N_4: a first-principles study

Sinan Li[a], Shaobin Yang[*b], Ding Shen[a], Wen Sun[b], Xueying Shan[b], Wei Dong[b], Yuehui Chen[c], Xu Zhang[b], Yongqiang Mao[c], Shuwei Tang[d]

[a] *College of Mining Engineering, Liaoning Technical University, Fuxin123000, PR China*

[b] *College of Materials Science and Engineering, Liaoning Technical University, Fuxin123000, PR China*

[c] *College of Science, Liaoning Technical University, Fuxin 123000, P R China*

[d] *Institute of Functional Material Chemistry, Faculty of Chemistry, Northeast Normal University, Changchun 130024, PR China*

*Corresponding Author: yangshaobin@lntu.edu.cn (Shaobin Yang)

Structures and relative energies of metastable bi-C_3N_4

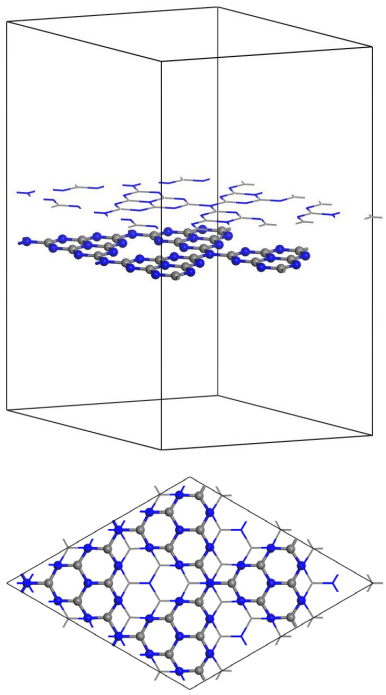

E = + 0.248 eV/super-cell

Figure S1. The optimized structure and relative energy of a metastable bi-C_3N_4. The bottom layer is plotted with balls, and the top layer is represented with sticks. The C and N atoms are denoted by gray and blue balls, respectively.

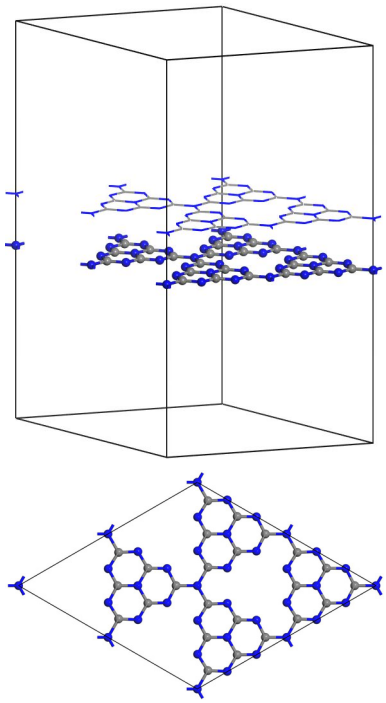

E = 1.985 eV/super-cell

Figure S2. The optimized structure of the bi-C_3N_4 with AA stacking. The bottom layer is plotted with balls, and the top layer is represented with sticks. The C and N atoms are denoted by gray and blue balls, respectively.

Isolated Li atom intercalation in the bi-C_3N_4

Table S1 shows the binding energies (E_b) of lithium polysulfides (LiPSs: Li_2S_n, n=1, 2, 4, and 8) and the structure (Li@bi-C_3N_4) of Li inserted in bi-C_3N_4.

The binding energy per Li (E_b^{LiPSs}) of LiPSs is defined as:

$$E_b^{LiPSs} = \left(n \cdot E_{S_8}/8 + 2E_{Li} - E_{LiPSs}\right)/2 \quad \text{(S1)}$$

where E_{S_8}, E_{Li} and E_{LiPSs} are the total energies of a S_8 molecule, per Li atom in bulk Li unit cell and LiPSs clusters, respectively.

The binding energy per Li ($E_b^{Li@bi\text{-}C_3N_4}$) of Li@bi-$C_3N_4$ is defined as:

$$E_b^{Li@bi\text{-}C_3N_4} = \left(E_{bi\text{-}C_3N_4} + 2E_{Li} - E_{Li@bi\text{-}C_3N_4}\right)/2 \quad \text{(S2)}$$

where $E_{bi\text{-}C_3N_4}$ and $E_{Li@bi\text{-}C_3N_4}$ are the total energies of bi-C_3N_4 and Li@bi-C_3N_4, respectively. The optimized structures of Li@bi-C_3N_4 is shown in Figure S3.

Table S1. The binding energies (E_b) of LiPSs and Li@bi-C_3N_4

	Li_2S_8	Li_2S_6	Li_2S_4	Li_2S_2	Li_2S	Li@bi-C_3N_4
E_b / eV	1.219	1.245	1.043	0.528	0.007	5.839

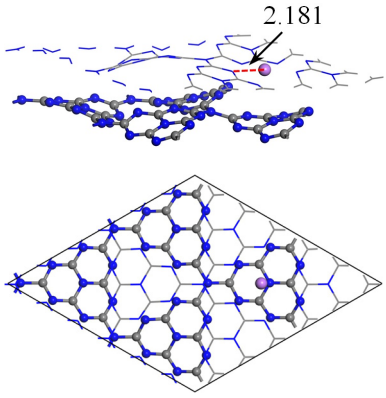

Figure S3. The optimized structure of the bi-C_3N_4 inserted by isolated Li atom. The bottom layer is plotted with balls, and the top layer is represented with sticks. The C, N and Li atoms are denoted by gray, blue and purple balls, respectively.

Charge density differences for S_8 and LiPSs

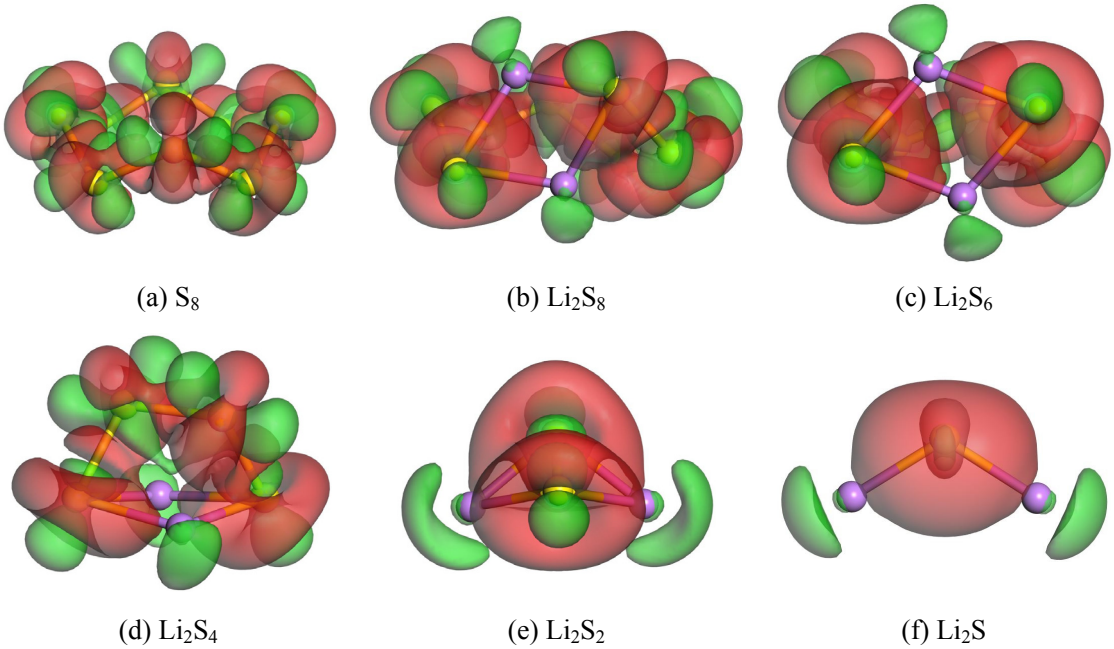

Figure S4. Isosurfaces for the intercalation structures of S_8 and LiPSs. The green and the red isosurfaces represent the regions of electron density loss and gain 0.02 e/Å^3, respectively. The S and Li atoms are denoted by yellow, purple balls, respectively.

The structures of the typically used ether solvents

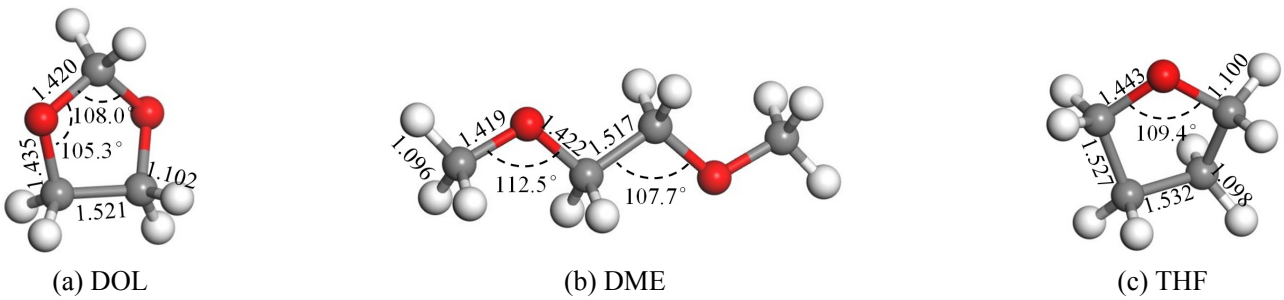

Figure S5. The optimized structures of three typically used 1,3-dioxolane (DOL), 1,2-dimethox-yethane (DME) and tetrahydrofuran (THF) ether solvents in liquid Li-S battery electrolytes, respectively. The C, H and O atoms are denoted by gray, white and red balls, respectively.

The structure of S_8 intercalation in the bilayer graphene

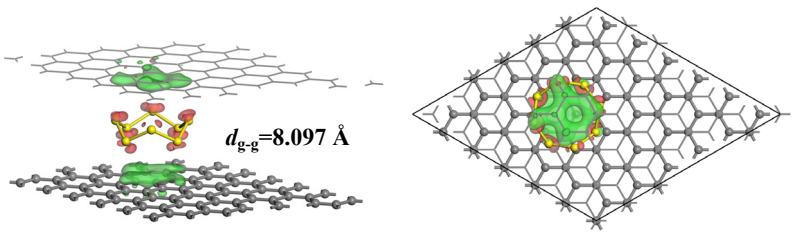

Figure S6. Isosurfaces for the pristine bilayer graphene inserted by S_8. The green and the red isosurfaces represent the regions of electron density loss and gain 0.001 e/Å^3, respectively. The C and S atoms are denoted by gray and yellow balls, respectively.

The structure of S_8 adsorption on the monolayer g-C_3N_4

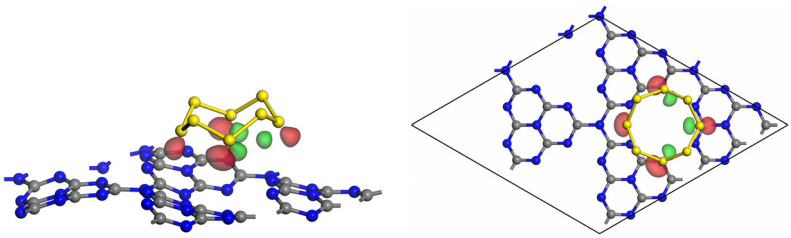

Figure S7. Isosurfaces for the structure of S_8 adsorption on the surface of monolayer g-C_3N_4. The green and the red isosurfaces represent the regions of electron density loss and gain 0.003 e/Å^3, respectively. The C, N and S atoms are denoted by gray, blue and yellow balls, respectively.

Cohesive energies for bi-C_3N_4 with different interlayer distances

Figure S8 shows the cohesive energy E_c as a function of the initial interlayer distances d_0 for bi-C_3N_4 with AB stacking, E_c can be defined by:

$$E_c = E_{\text{bi-C}_3\text{N}_4} - 2 \cdot E_{\text{mono-C}_3\text{N}_4} \tag{S3}$$

where $E_{\text{bi-C}_3\text{N}_4}$ are the total energies of the bi-C_3N_4 with AB stacking; $E_{\text{mono-C}_3\text{N}_4}$ is the total energy of monolayer g-C_3N_4 (mono-C_3N_4).

As shown in Figure S8, when the interlayer distance is larger than 8.0 Å, the E_c are close to 0 eV indicating a negligible vdW attraction between the double layers of bi-C_3N_4.

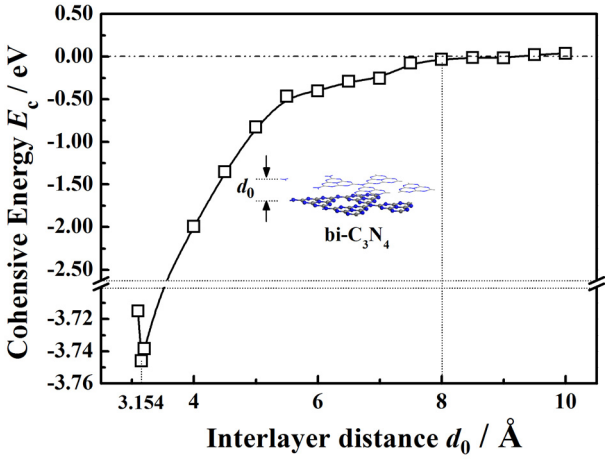

Figure S8. Cohesive energies E_c as a function of the initial interlayer distances d_0 for bi-C_3N_4 with AB stacking.

Details of the structure optimizing for the LiPSs and solvent molecules inserted structures

In order to obtain the ground states of LiPSs and solvent molecules inserted structures (S_8@bi-C_3N_4, LiPSs@bi-C_3N_4, DME@bi-C_3N_4, THF@bi-C_3N_4 and DOL@bi-C_3N_4), the initial geometries of the inserted structures were generated by the process below.

1st step: testing the interlayer distances

The single point energies ($E_{X@bi-C_3N_4}$) of S_8@bi-C_3N_4 and DME/DOL/THF@bi-C_3N_4 with different $d_{g\text{-}g}$ were calculated to test the effects of interlayer distances $d_{g\text{-}g}$ on the total energies of LiPSs@bi-C_3N_4 and Solvents@bi-C_3N_4, respectively. A cutoff energy of 500 eV and a Monkhorst-Pack k-point mesh of 2 × 2 ×1 are used. The convergence threshold for self-consistent field (SCF) tolerance is set to 1.0×10^{-6} eV/atom. Figure S9 shows the relative energies E_r as a function of $d_{g\text{-}g}$ for S_8@bi-C_3N_4 and Solvents@bi-C_3N_4. E_r is defined by :

$$E_r = E_{X@bi-C_3N_4} - E^{min}_{X@bi-C_3N_4} \tag{S4}$$

where $E^{min}_{X@bi-C_3N_4}$ are the minimum value in $E_{X@bi-C_3N_4}$. The results show that E_r are the smallest ones (defined by 0 eV/super-cell) when the $d_{g\text{-}g}$ are 8.0 Å and 7.0 Å for S_8@bi-C_3N_4 and Solvents@bi-C_3N_4, respectively.

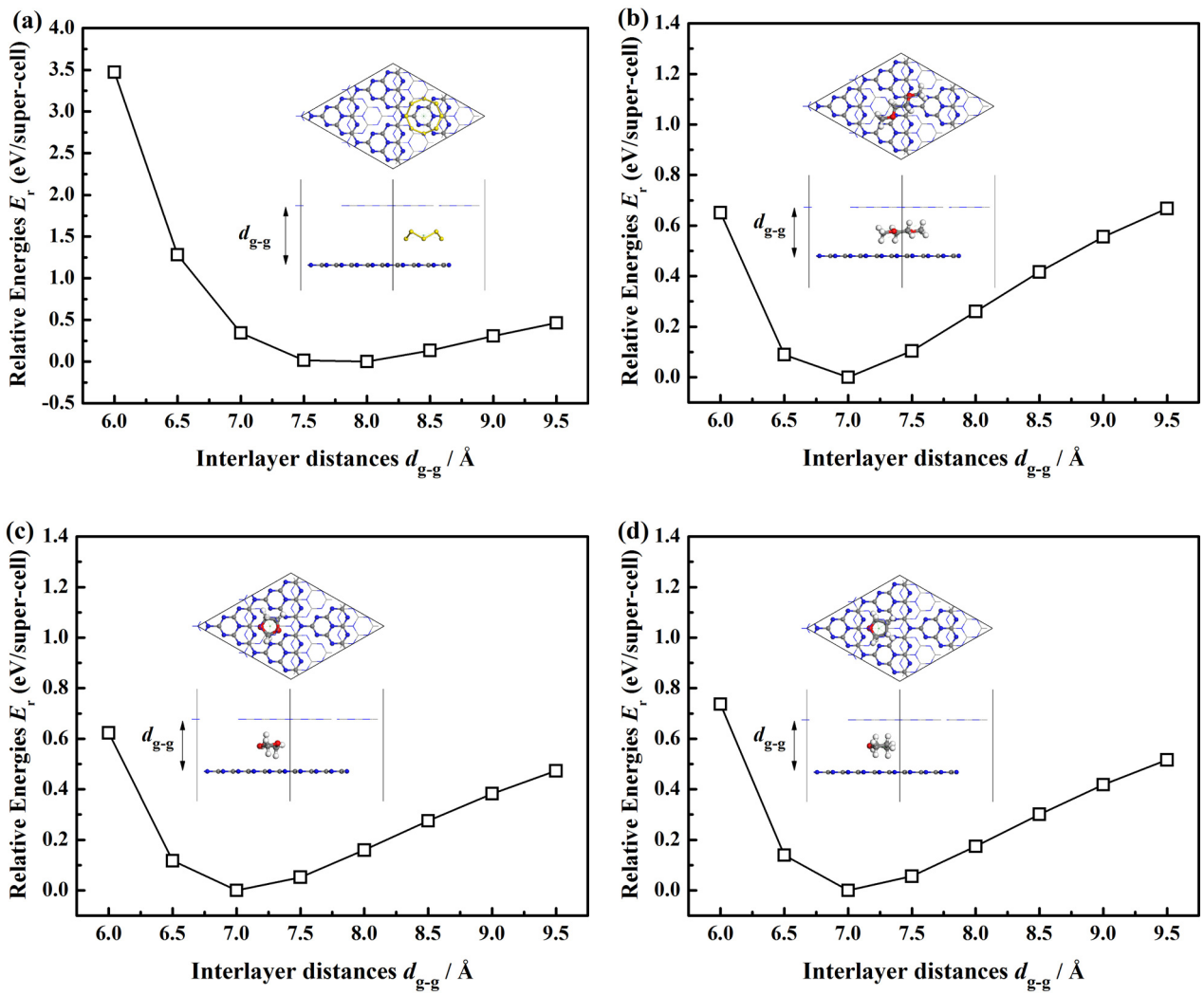

Figure S9. Relative energies E_r as a function of the interlayer distances $d_{g\text{-}g}$ for (a) S_8@bi-C_3N_4, (b) DME@bi-C_3N_4, (c) DOL@bi-C_3N_4 and (d) THF@bi-C_3N_4

2nd step: testing the loading sites in the interlayer

As shown in Figure S10, based on the tests for $d_{g\text{-}g}$, the centers of mass for S_8 and LiPSs clusters were loaded at the three sites in bi-C_3N_4 with $d_{g\text{-}g}$=8.0 Å, and two sites (No.1 and 3) were tested for DME/DOL/THF loaded in bi-C_3N_4 with $d_{g\text{-}g}$=7.0 Å. From Table S2 to S10 show structures and relative energies *E* for S8, LiPSs, DME, DOL and THF loaded at different sites and with different the rotation angles in bi-C_3N_4, respectively. A cutoff energy of 500 eV and a Monkhorst-Pack k-point mesh of 2 × 2 ×1 are used to calculate the single point energies. The convergence threshold for self-consistent field (SCF) tolerance is set to 1.0×10^{-6} eV/atom.

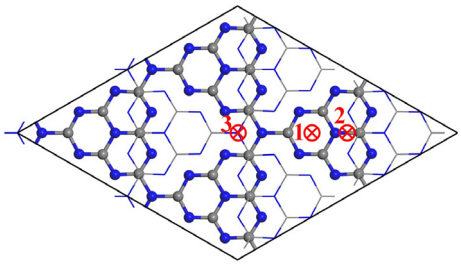

Figure S10. Tested sites for LiPSs in the interlayer of bi-C_3N_4

3rd step: optimizing with medium quality

Based on the results in Table S2~S10, the structures with the smallest *E* for each loading site were optimized with medium quality. A cutoff energy of 270 eV is used for S_8@bi-C_3N_4 and LiPSs@bi-C_3N_4, and 300 eV is used for DME/DOL/THF@bi-C_3N_4. A Monkhorst-Pack k-point mesh is 2 × 2 × 1. The convergence threshold for self-consistent field (SCF) tolerance is set to 2.0×10^{-5} eV/atom. Atomic positions are relaxed with the maximum force on all atoms to be less than 0.05 eV/Å. The maximum displacement is 2.0×10^{-3} Å, and the stress is less than 0.1 GPa. The *E* of optimized structures are listed in Table S11~S19.

The last step: optimizing with fine quality

Based on the results in Table S11~S19, one structure with the smallest *E* (highlighted one) was optimized with fine quality for S_8@bi-C_3N_4, LiPSs@bi-C_3N_4, DME@bi-C_3N_4, DOL@bi-C_3N_4 and THF@bi-C_3N_4, respectively. A cutoff energy of 500 eV and a Monkhorst-Pack k-point mesh of 2 × 2 ×1 are used. The convergence threshold for self-consistent field (SCF) tolerance was set to 1.0×10^{-6} eV/atom. Atomic positions are relaxed with the maximum force on all atoms to be less than 0.03 eV/Å. The maximum displacement is 1.0×10^{-3} Å, and the stress is less than 0.05 GPa.

Table S2. Relative energies *E* as a function of the loading sites and the rotation for S_8@bi-C_3N_4

	Site No. 1	Site No. 2	Site No. 3
Rot. 1	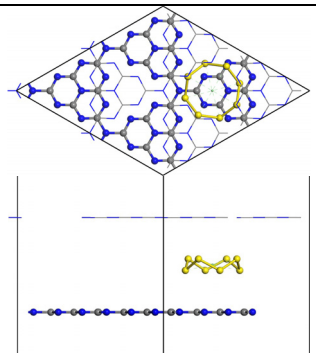 S_8-1-R1	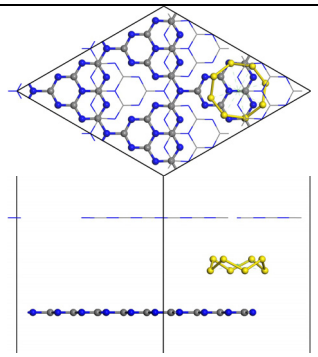 S_8-2-R1	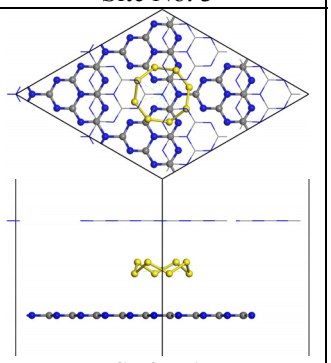 S_8-3-R1
E (eV/super-cell)	0.076	0.006	0.029
Rot. 2	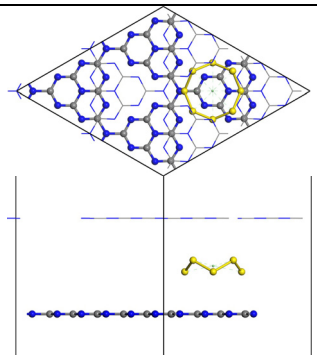 S_8-1-R2	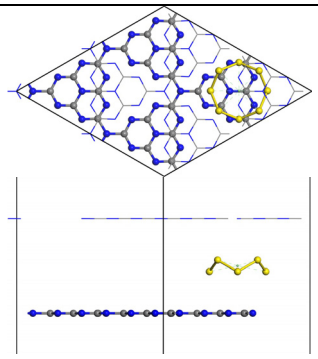 S_8-2-R2	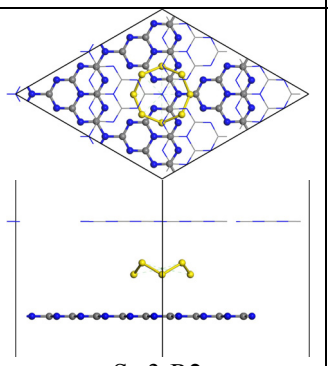 S_8-3-R2
E (eV/super-cell)	0.073	0.000	0.014

Table S3. Relative energies *E* as a function of the loading sites and the rotation for Li_2S_8@bi-C_3N_4

	Site No. 1	Site No. 2	Site No. 3
Rot. 1	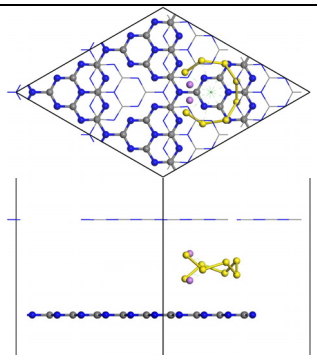 Li_2S_8-1-R1	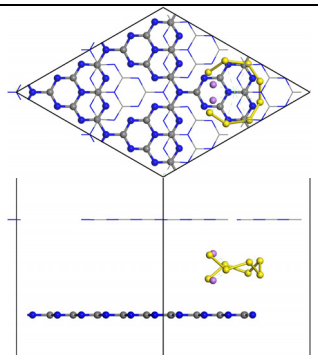 Li_2S_8-2-R1	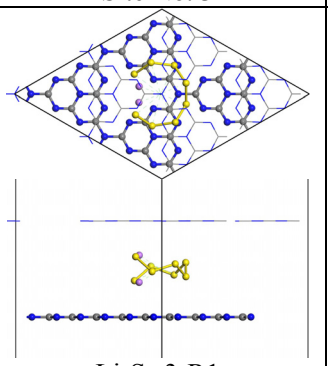 Li_2S_8-3-R1
E (eV/super-cell)	0.360	0.236	0.273
Rot. 2	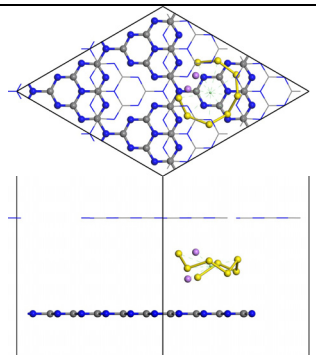 Li_2S_8-1-R2	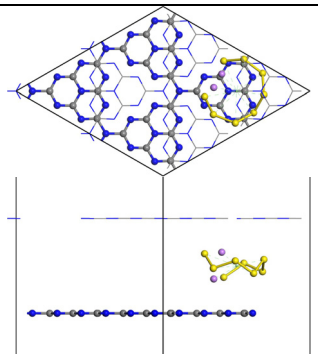 Li_2S_8-2-R2	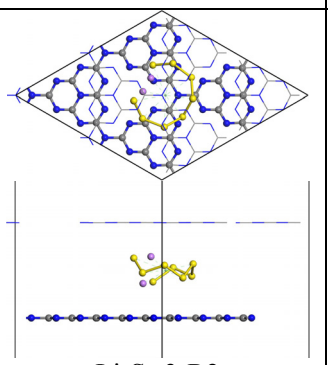 Li_2S_8-3-R2
E (eV/super-cell)	0.446	0.327	0.000

Rot. 3	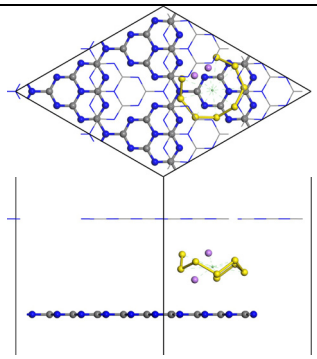 Li_2S_8-1-R3	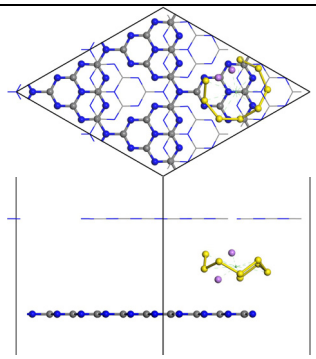 Li_2S_8-2-R3	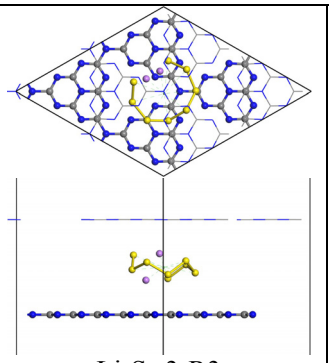 Li_2S_8-3-R3
E (eV/super-cell)	0.295	0.352	0.153

Table S4. Relative energies *E* as a function of the loading sites and the rotation for Li_2S_6@bi-C_3N_4

	Site No. 1	Site No. 2	Site No. 3
Rot. 1	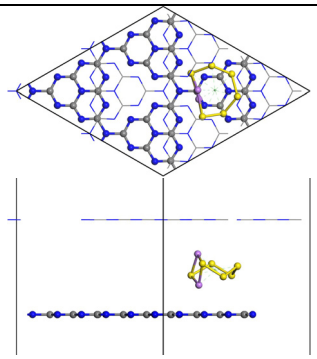 Li_2S_6-1-R1	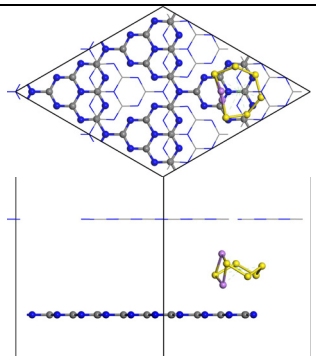 Li_2S_6-2-R1	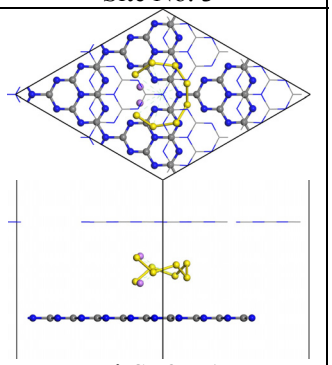 Li_2S_6-3-R1
E (eV/super-cell)	0.193	0.366	0.150
Rot. 2	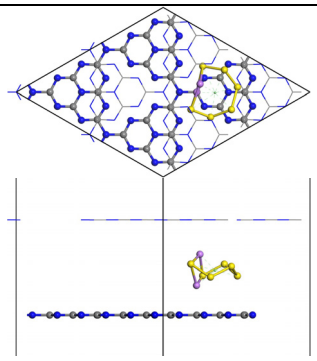 Li_2S_6-1-R2	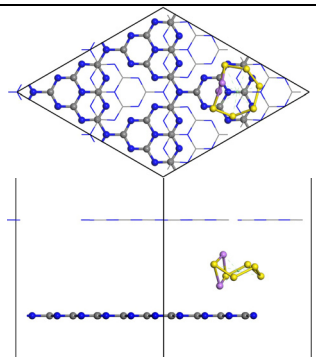 Li_2S_6-2-R2	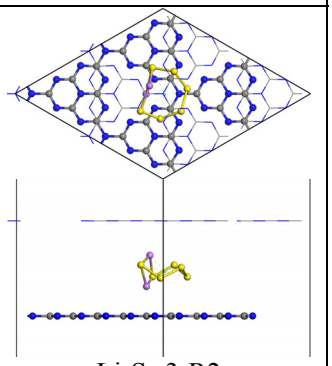 Li_2S_6-3-R2
E (eV/super-cell)	0.300	0.417	0.000
Rot. 3	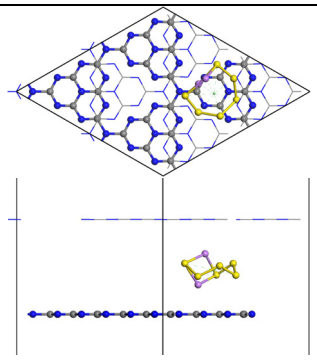 Li_2S_6-1-R3	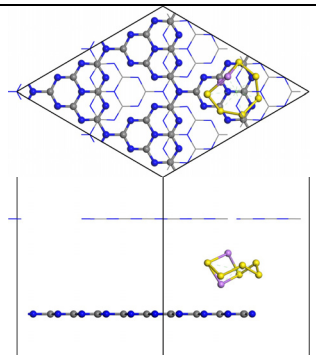 Li_2S_6-2-R3	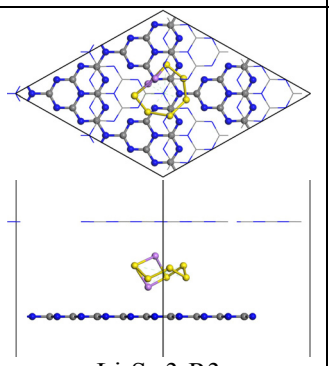 Li_2S_6-3-R3
E (eV/super-cell)	0.249	0.388	0.012

Table S5. Relative energies *E* as a function of the loading sites and the rotation for Li_2S_4@bi-C_3N_4

	Site No. 1	Site No. 2	Site No. 3
Rot. 1	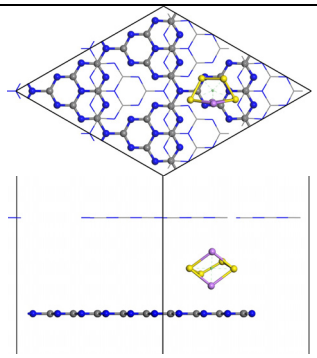 Li_2S_4-1-R1	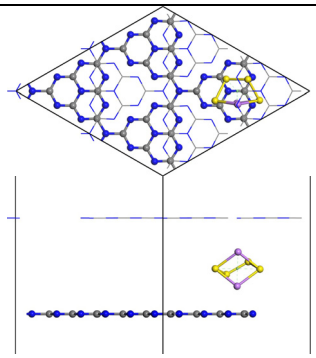 Li_2S_4-2-R1	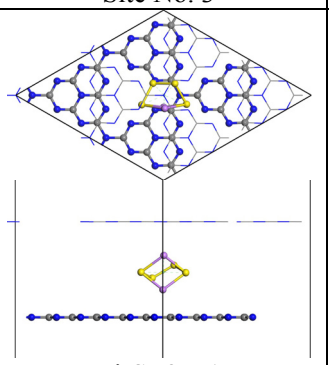 Li_2S_4-3-R1
E (eV/super-cell)	0.188	0.606	0.476
Rot. 2	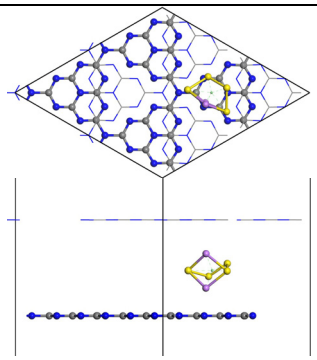 Li_2S_4-1-R2	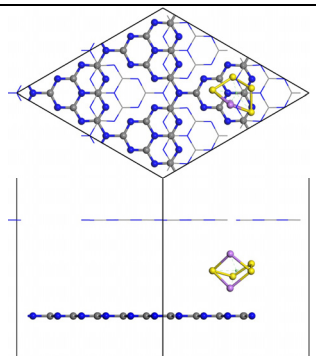 Li_2S_4-2-R2	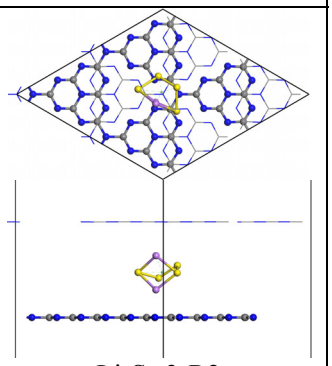 Li_2S_4-3-R2
E (eV/super-cell)	0.138	0.479	0.202
Rot. 3	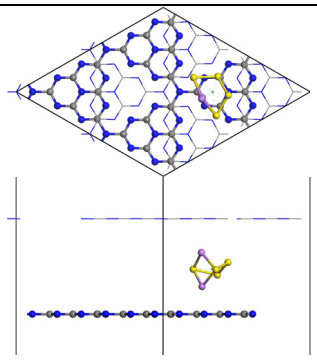 Li_2S_4-1-R3	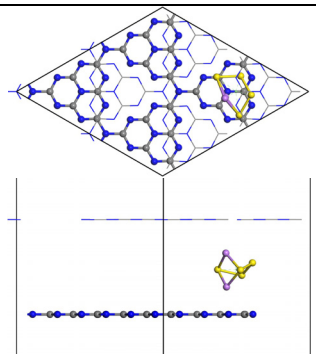 Li_2S_4-2-R3	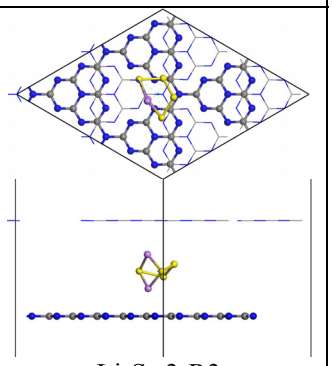 Li_2S_4-3-R3
E (eV/super-cell)	0.220	0.437	0.000
Rot. 4	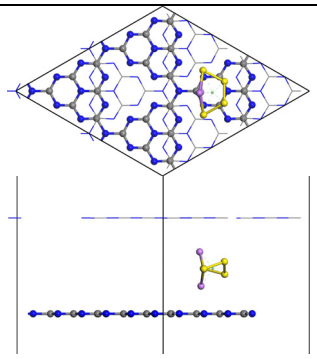 Li_2S_4-1-R4	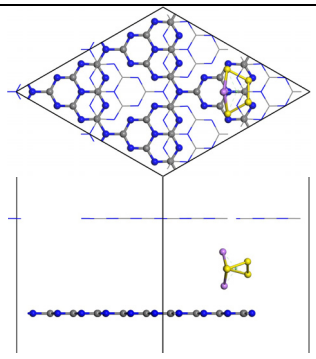 Li_2S_4-2-R4	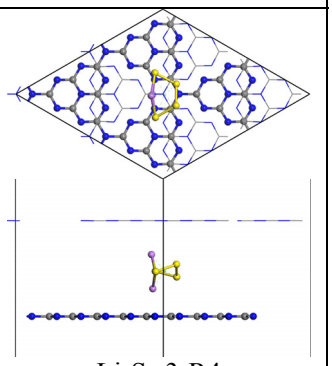 Li_2S_4-3-R4
E (eV/super-cell)	0.316	0.498	0.014

Table S6. Relative energies *E* as a function of the loading sites and the rotation for Li_2S_2@bi-C_3N_4

	Site No. 1	Site No. 2	Site No. 3
Rot. 1	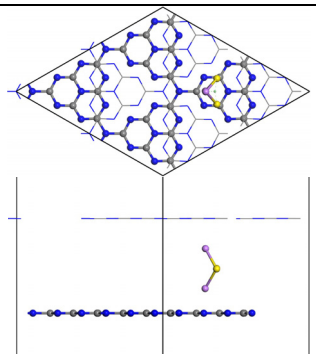 Li_2S_2-1-R1	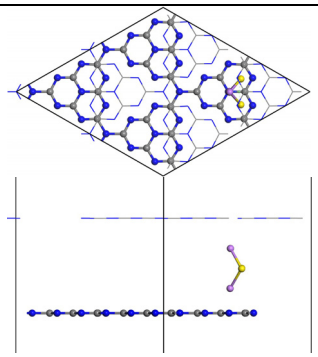 Li_2S_2-2-R1	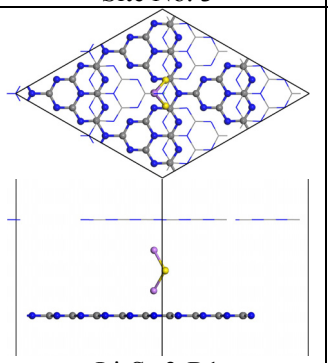 Li_2S_2-3-R1
E (eV/super-cell)	0.265	0.647	0.000
Rot. 2	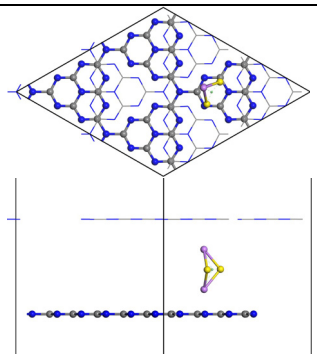 Li_2S_2-1-R2	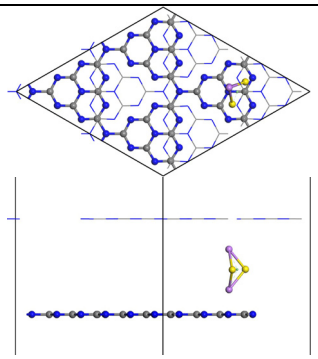 Li_2S_2-2-R2	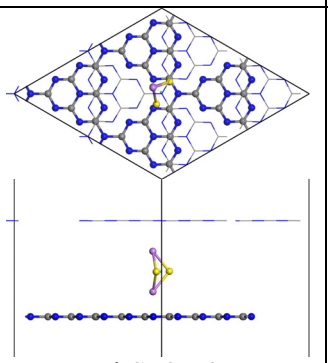 Li_2S_2-3-R2
E (eV/super-cell)	0.212	0.590	0.077
Rot. 3	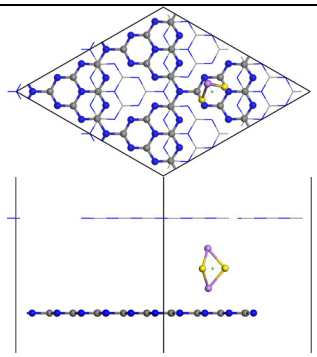 Li_2S_2-1-R3	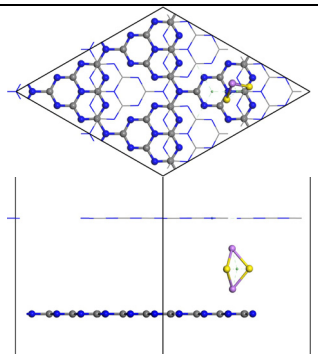 Li_2S_2-2-R3	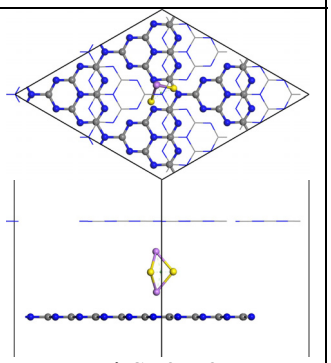 Li_2S_2-3-R3
E (eV/super-cell)	0.127	0.588	0.299
Rot. 4	--	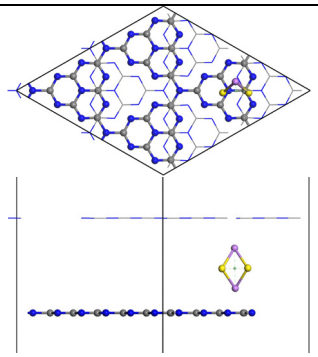 Li_2S_2-2-R4	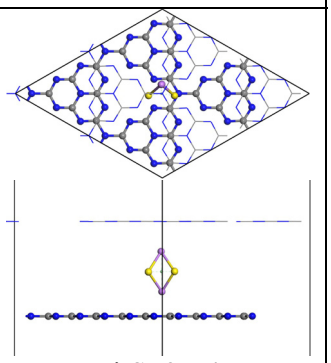 Li_2S_2-3-R4
E (eV/super-cell)	--	0.638	0.522

Table S7. Relative energies *E* as a function of the loading sites and the rotation for Li_2S@bi-C_3N_4

	Site No. 1	Site No. 2	Site No. 3
Rot. 1	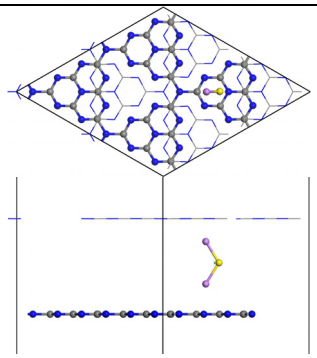 Li_2S-1-R1	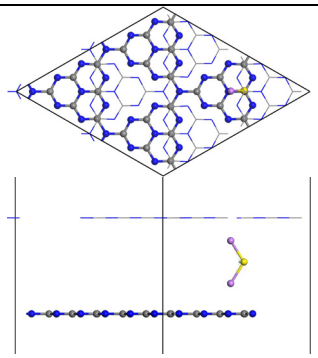 Li_2S-2-R1	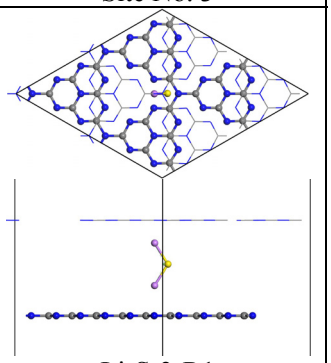 Li_2S-3-R1
E (eV/super-cell)	0.000	0.373	0.661
Rot. 2	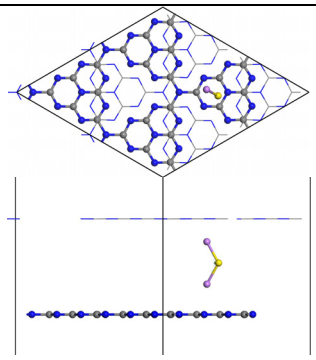 Li_2S-1-R2	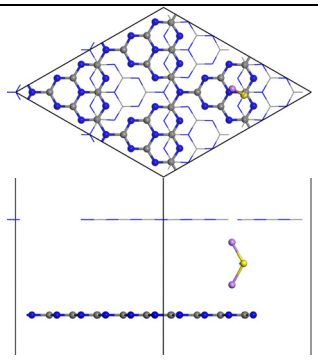 Li_2S-2-R2	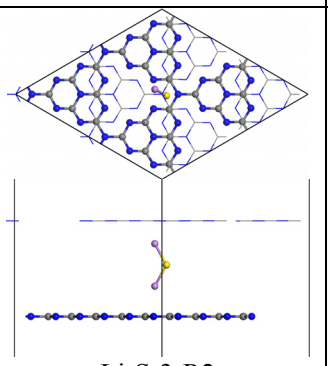 Li_2S-3-R2
E (eV/super-cell)	0.004	0.419	0.624
Rot. 3	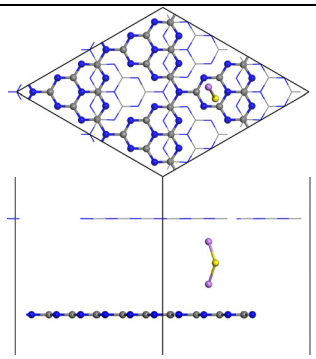 Li_2S-1-R3	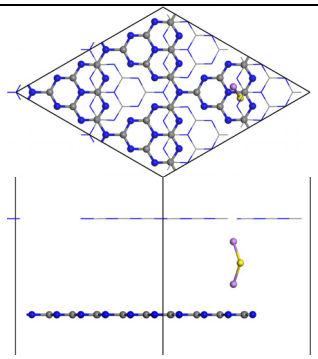 Li_2S-2-R3	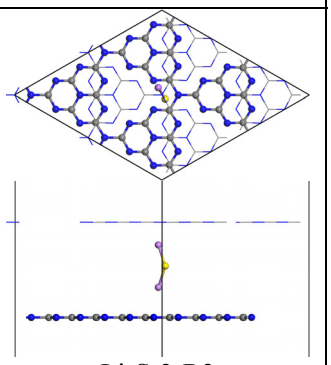 Li_2S-3-R3
E (eV/super-cell)	0.026	0.574	0.694
Rot. 4	--	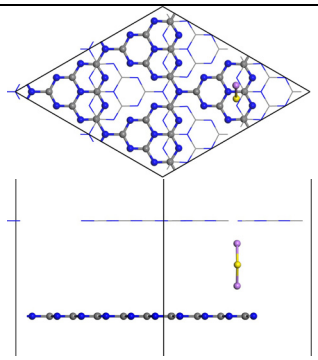 Li_2S-2-R4	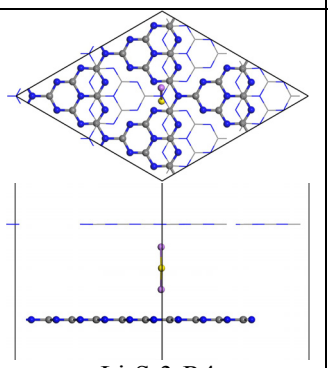 Li_2S-3-R4
E (eV/super-cell)	--	0.803	0.818

Table S8. Relative energies *E* as a function of the loading sites and the rotation for DME@bi-C_3N_4

	Site No. 1	Site No. 2	Site No. 3
Rot. 1	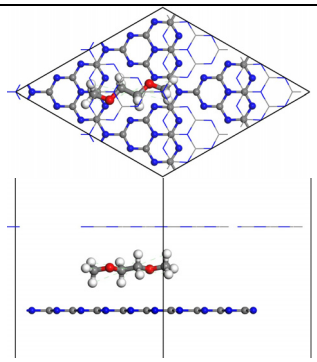 DME-1-R1	--	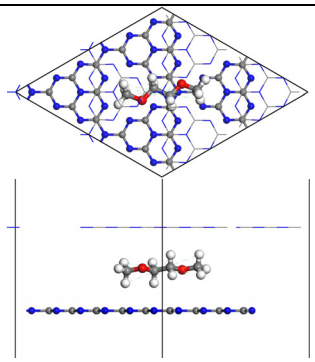 DME-3-R1
E (eV/super-cell)	0.199	--	0.000
Rot. 2	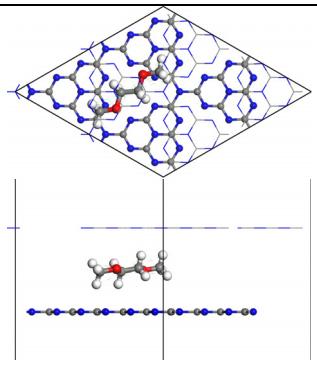 DME-1-R2	--	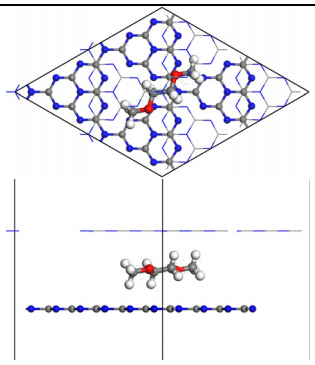 DME-3-R2
E (eV/super-cell)	0.238	--	0.063
Rot. 3	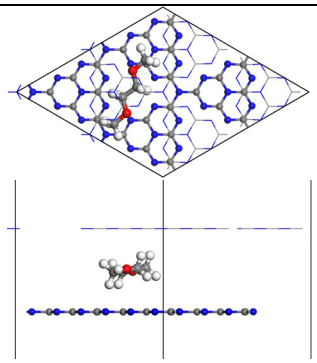 DME-1-R3	--	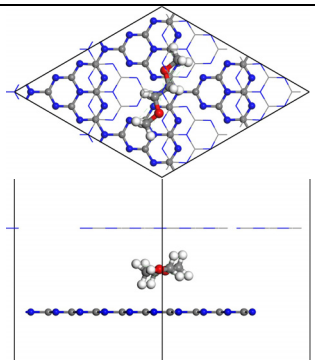 DME-3-R3
E (eV/super-cell)	0.134	--	0.163
Rot. 4	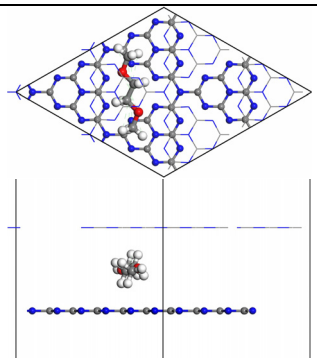 DME-1-R4	--	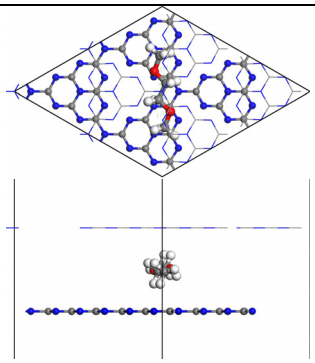 DME-3-R4
E (eV/super-cell)	0.102	--	0.233

Table S9. Relative energies *E* as a function of the loading sites and the rotation for DOL@bi-C_3N_4

	Site No. 1	Site No. 2	Site No. 3
Rot. 1	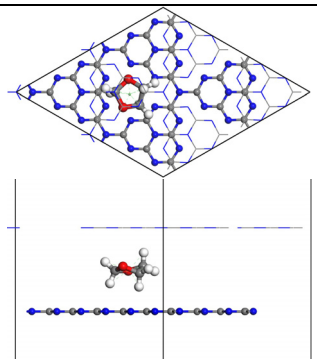 DOL-1-R1	--	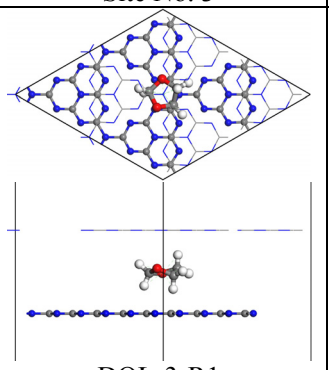 DOL-3-R1
E (eV/super-cell)	0.132	--	0.134
Rot. 2	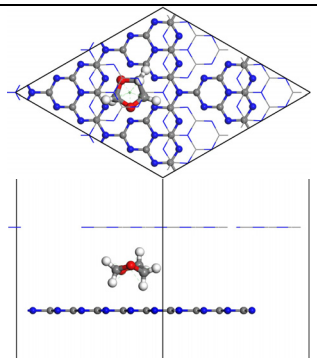 DOL-1-R2	--	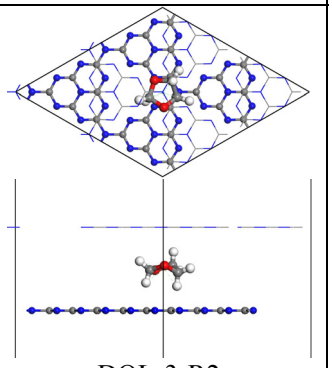 DOL-3-R2
E (eV/super-cell)	0.086	--	0.219
Rot. 3	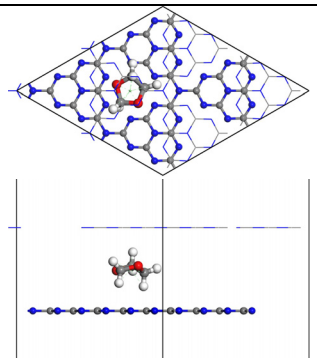 DOL-1-R3	--	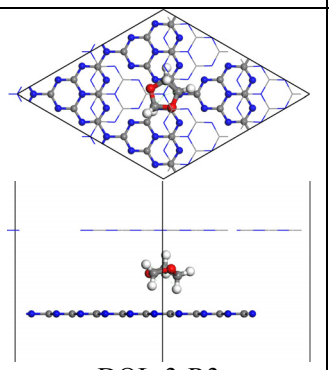 DOL-3-R3
E (eV/super-cell)	0.024	--	0.290
Rot. 4	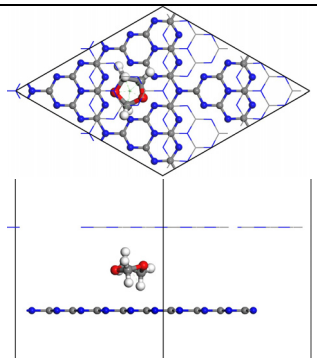 DOL-1-R4	--	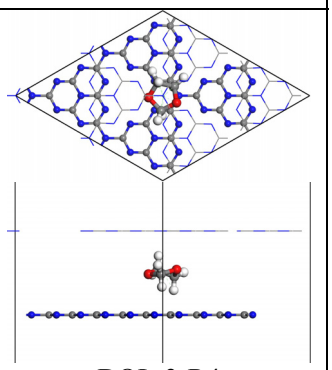 DOL-3-R4
E (eV/super-cell)	0.000	--	0.313

Table S10. Relative energies *E* as a function of the loading sites and the rotation for THF@bi-C_3N_4

	Site No. 1	Site No. 2	Site No. 3
Rot. 1	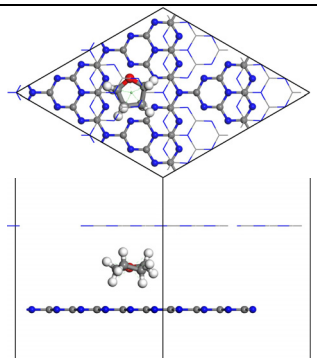 THF-1-R1	-- --	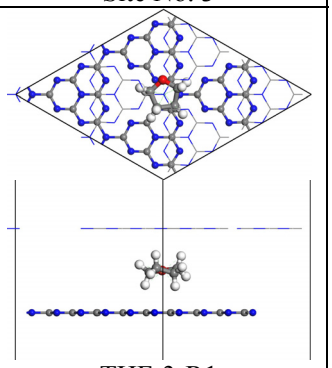 THF-3-R1
E (eV/super-cell)	0.136		0.062
Rot. 2	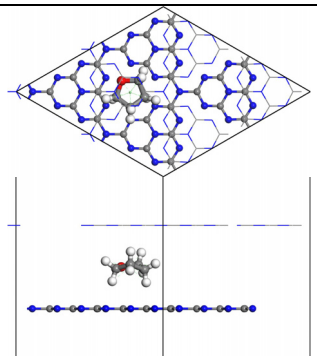 THF-1-R2	-- --	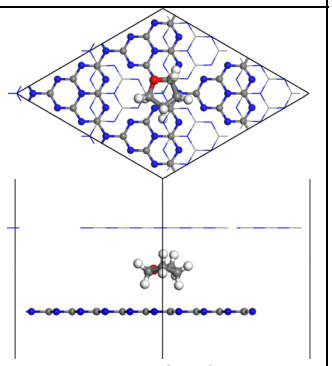 THF-3-R2
E (eV/super-cell)	0.062		0.192
Rot. 3	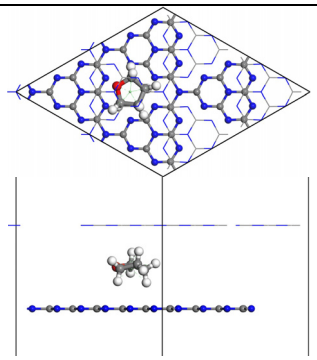 THF-1-R3	-- --	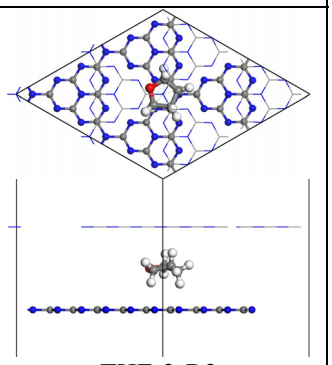 THF-3-R3
E (eV/super-cell)	0.000		0.267
Rot. 4	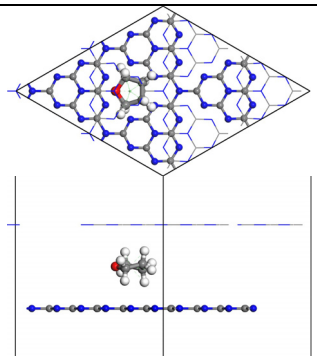 THF-1-R4	-- --	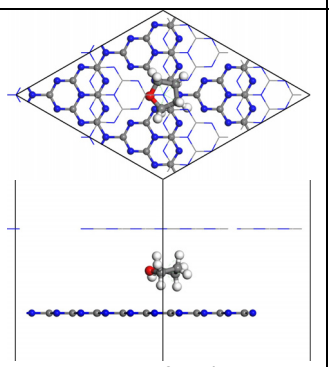 THF-3-R4
E (eV/super-cell)	0.021		0.213

Table S11. Relative energies *E* and optimized structures for optimized S_8-1-R2, S_8-2-R2 and S_8-3-R2 with medium quality

	Site No. 1	Site No. 2	Site No. 3
Structures after optimization with medium quality	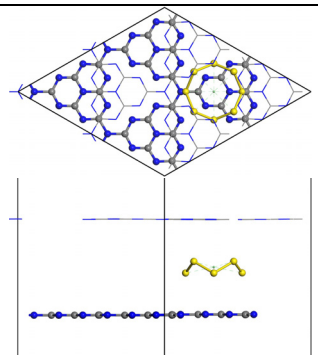 S_8-1-R2	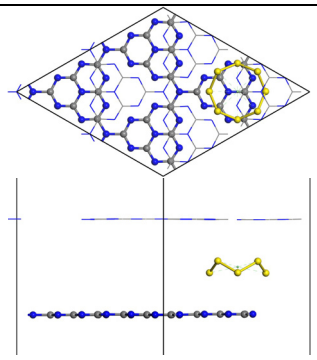 S_8-2-R2	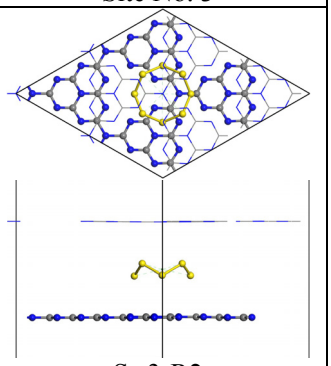 S_8-3-R2
E (eV/super-cell)	0.000	0.150	0.178

Table S12. Relative energies *E* and optimized structures for optimized Li_2S_8-1-R3, Li_2S_8-2-R1 and Li_2S_8-3-R2 with medium quality

	Site No. 1	Site No. 2	Site No. 3
Structures after optimization with medium quality	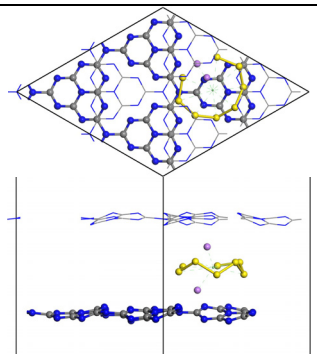 Li_2S_8-1-R3	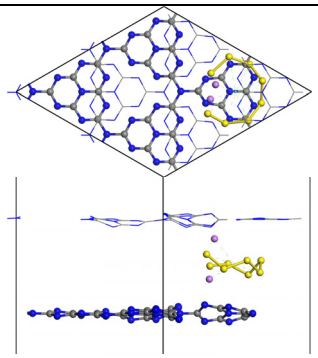 Li_2S_8-2-R1	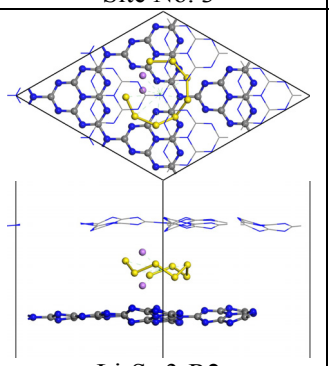 Li_2S_8-3-R2
E (eV/super-cell)	0.150	1.070	0.000

Table S13. Relative energies *E* and optimized structures for optimized Li_2S_6-1-R1, Li_2S_6-2-R1 and Li_2S_6-3-R2 with medium quality

	Site No. 1	Site No. 2	Site No. 3
Structures after optimization with medium quality	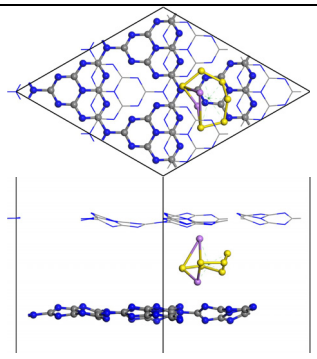 Li_2S_6-1-R1	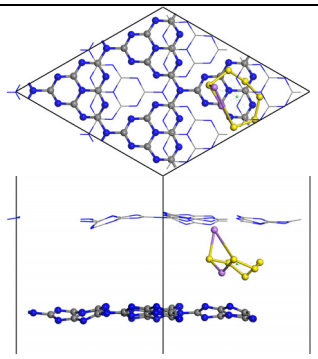 Li_2S_6-2-R1	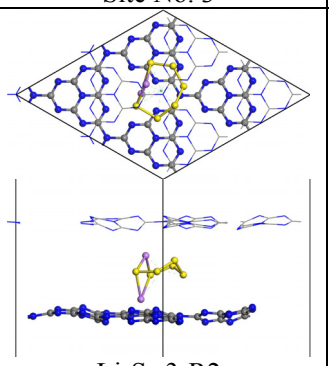 Li_2S_6-3-R2
E (eV/super-cell)	0.019	0.433	0.000

Table S14. Relative energies *E* and optimized structures for optimized Li_2S_4-1-R2, Li_2S_4-2-R3 and Li_2S_4-3-R3 with medium quality

	Site No. 1	Site No. 2	Site No. 3
Structures after optimization with medium quality	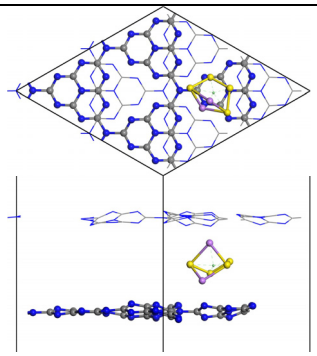 Li_2S_4-1-R2	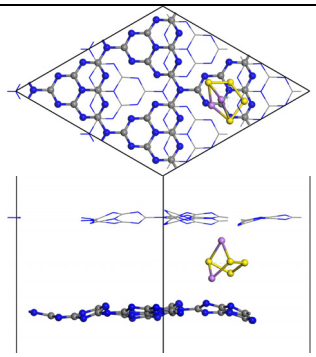 Li_2S_4-2-R3	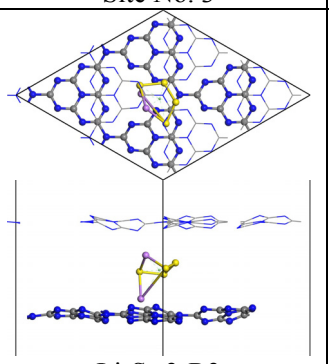 Li_2S_4-3-R3
E (eV/super-cell)	0.245	0.471	0.000

Table S15. Relative energies *E* and optimized structures for optimized Li_2S_2-1-R3, Li_2S_2-2-R3 and Li_2S_2-3-R1 with medium quality

	Site No. 1	Site No. 2	Site No. 3
Structures after optimization with medium quality	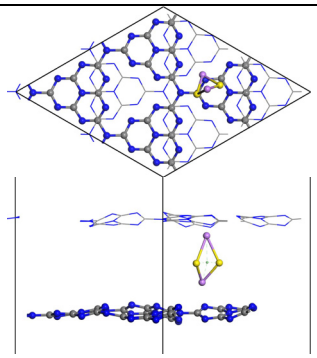 Li_2S_2-1-R3	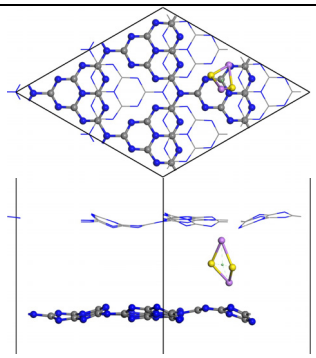 Li_2S_2-2-R3	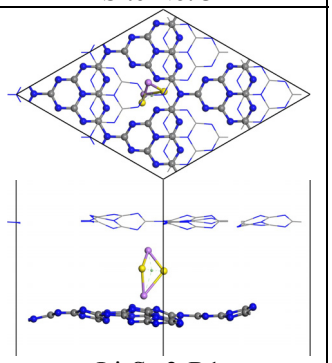 Li_2S_2-3-R1
E (eV/super-cell)	0.145	0.187	0.000

Table S16. Relative energies *E* and optimized structures for optimized Li_2S-1-R1, Li_2S-2-R1 and Li_2S-3-R2 with medium quality

	Site No. 1	Site No. 2	Site No. 3
Structures after optimization with medium quality	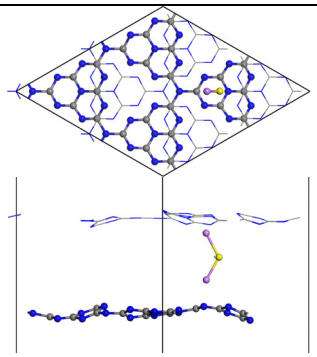 Li_2S-1-R1	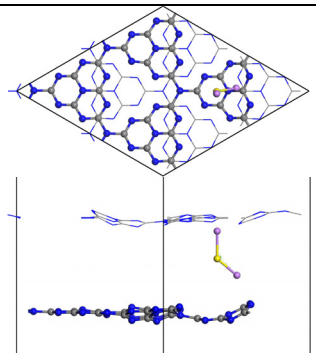 Li_2S-2-R1	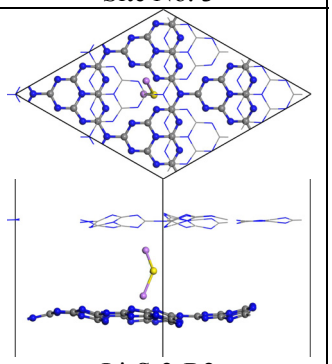 Li_2S-3-R2
E (eV/super-cell)	0.602	0.780	0.000

Table S17. Relative energies *E* and optimized structures for optimized DME-1-R1 and DME-3-R2 with medium quality

	Site No. 1	Site No. 2	Site No. 3
Structures after optimization with medium quality	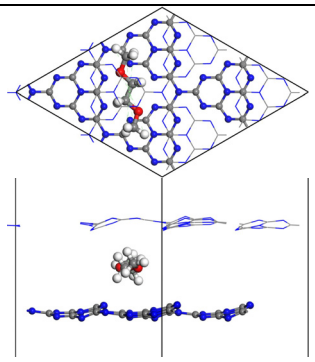 DME-1-R1	--	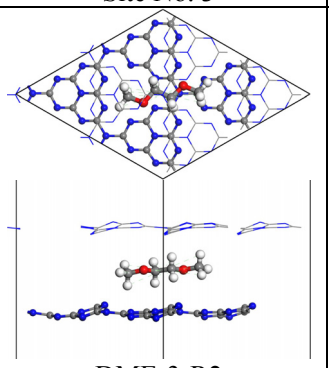 DME-3-R2
E (eV/super-cell)	0.000	--	0.012

Table S18. Relative energies *E* and optimized structures for optimized DOL-1-R1 and DOL-3-R1 with medium quality

	Site No. 1	Site No. 2	Site No. 3
Structures after optimization with medium quality	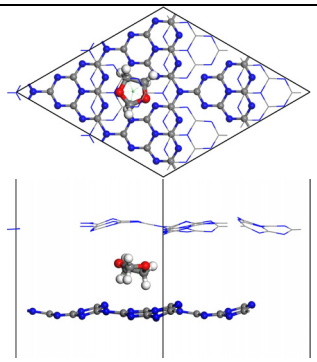 DOL-1-R1	--	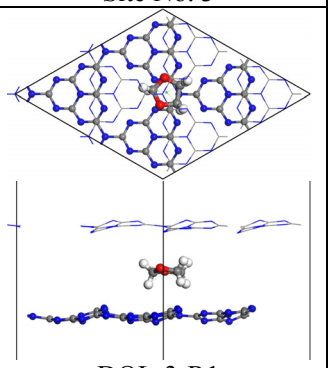 DOL-3-R1
E (eV/super-cell)	0.000	--	0.662

Table S19. Relative energies *E* and optimized structures for optimized THF-1-R3 and THF-3-R1 with medium quality

	Site No. 1	Site No. 2	Site No. 3
Structures after optimization with medium quality	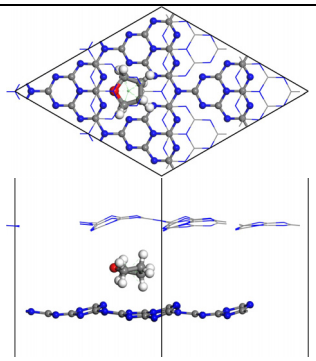 THF-1-R3	--	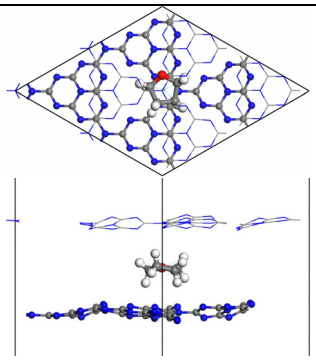 THF-3-R1
E (eV/super-cell)	0.000	--	0.059